

The Structure of Alkanethiol Films on Liquid Mercury: An X-Ray Study

M. DEUTSCH¹, O. M. MAGNUSSEN^{2*}, B. M. OCKO², M. J. REGAN^{3†},
AND P. S. PERSHAN³

¹Physics Dept., Bar-Ilan University, Ramat-Gan 52900, Israel. ²Physics Dept., Brookhaven National Laboratory, Upton, New York, ³Div. of Applied Science & Physics Dept., Harvard University, Cambridge, Massachusetts

6.1 Introduction.....	180
6.2 Experimental.....	185
6.2.1 Samples and Sample Cell.....	185
6.2.2 Surface X-ray Measuring Techniques.....	186
6.2.3 Modeling and Fitting.....	186
6.3 Results.....	188
6.3.1 Monolayers.....	188
Reflectivity.....	188
GIXD.....	192
6.3.2 Multilayers.....	193
Reflectivity.....	193
GIXD.....	197
6.4 Discussion.....	198
6.5 Conclusion.....	200

*Present address: Abt. Oberflächenchemie u. Katalyse, Universität Ulm, D-89069 Ulm, Germany.

†Present address: Hewlett-Packard, IJBU Advanced Research Lab, Corvallis, OR 97330, U.S.A.

Abstract

Alkanethiol monolayers on the surface of liquid mercury are a class of supported organic films intermediate between the limiting cases of Langmuir monolayers (LAMs) on water and self-assembled organic monolayers (SAMs) on crystalline substrates. We review here the first Å-resolution studies of their structure, using synchrotron-based surface-specific X-ray techniques, for chain lengths of $8 < n < 30$. We show that well-defined monolayers and multilayers of alkanethiols can be prepared on the liquid mercury surface. The molecules in the layers are well aligned along the surface-normal direction and packed very densely at $\sim 19\text{Å}^2$ per molecule. Surprisingly, in spite of this high density, no long-range in-plane order is observed for the monolayer phase. By contrast, the multilayers—which consist of stacks of thiol bilayers intercalated with a mercury layer between the two thiol monolayers—show a long-range in-plane crystalline order, with an oblique two-dimensional unit cell and a coherence length of a few thousand Å. We discuss these results in terms of the relative strengths of the interchain and substrate-head group interactions in the system in each case and show why the dominance of the former establishes long-range order in the multilayers, while the dominance of the latter induces disorder in the monolayer phase.

6.1 Introduction

Layers of organic molecules on water were already known to the ancient Greeks,¹ Romans,² and Chinese,³ who observed that a stormy sea surface in the vicinity of a ship or a diver could be calmed down by pouring oil over the water. Benjamin Franklin⁴ realized, and demonstrated experimentally in the Clapham pools, that in spite of their strong effect on waves such layers are in fact very thin. Following the seminal work of I. Langmuir⁵ and K. B. Blodgett,⁶ these layers became to be known as Langmuir monolayers (LAMs in the following) when spread on water, and Langmuir-Blodgett films when transferred as monolayers or multilayers onto a solid substrate. These layers have been investigated by macroscopic methods, mostly surface pressure vs. area isotherms in so-called Langmuir troughs, for almost a century.⁷⁻⁹ However, due to the small number of molecules involved, as compared to bulk material, the study of their structure *at a molecular level* by X-ray techniques was not feasible until about a decade ago, when sophisticated surface-sensitive X-ray scattering techniques suitable for liquid surfaces were developed,¹⁰ and the first studies of LAMs on water were published.¹¹ These techniques rely heavily on the intense,

highly collimated X-ray beams available at synchrotron sources, as well as on sophisticated mathematical modeling and computer fitting methods. Over the last decade, these techniques proved extremely successful in elucidating the structures of many types of LAMs—such as straight-chain surfactants¹² (fatty acids, alcohols, alkanes, phospholipids, etc.), polymers of various shapes,¹³ fullerenes,¹⁴ etc.—and their variation with surface pressure, temperature, subphase additives, and other physical and chemical parameters. With very few exceptions,¹⁵ all of these structural studies were done on water subphases.

A different type of an organic overlayer, thus far applied exclusively to solid surfaces, has its origin in the work of Bigelow et al.¹⁶ and was later developed and extended by Netzer and Sagiv,¹⁷ Nuzzo and Allara,¹⁸ and others.⁸ These self-assembled monolayers (SAMs) are formed by adsorption from a solution of organic molecules onto the surface of a solid, poly- or single-crystalline metal or semiconductor immersed in the solution. Although the first SAMs employed alkyl trichlorosilanes on silicon surfaces, soon it was realized that alkyl thiols, sulfides, and disulfides yield denser, more reproducible, and more uniform SAMs on gold, silver, and copper single-crystal substrates through the strong metal-sulfur covalent bond. Thiol SAMs on various crystallographic facets of single gold crystals are by far the best-studied SAMs and are considered to be a model system.^{19,8,20}

Supported organic layers are of prime interest for many scientific disciplines for a variety of reasons. In physics, such layers represent quasi-two-dimensional matter and hence allow the study of the dimensional dependence of phase behavior, critical phenomena, and other fundamental physical effects. In biology, these monolayers serve as simplified models for the cell membrane and may provide information on biological processes involving the membrane. In chemistry, they aid in the study of crystal nucleation and growth, charge transfer, aggregation phenomena, colloid and emulsion chemistry, and much more. In medical science, these films have important roles in organ- and tissue-specific drug delivery, in controlled release of medication, and in immunology,²¹ where they render viral binding sites in cell membranes inactive.

Many applications, such as corrosion prevention, wear protection, biosensing, adhesion enhancement, etc., make these films highly important in industry as well. They hold also great promise for the field of electronics in the next millenium: By providing (in principle) the means for structural manipulation and control of matter *at the molecular level*, they may open the road to molecular-level miniaturization of electronic devices.

The structure and phase behavior of the two classes of organic monolayers discussed above are sensitively controlled by two competing interactions. The first of these is the interchain (IC) van der Waals interaction, for which the minimal-energy monolayer structure is one of densely packed parallel chains.

This interaction gives rise to crystalline layered structures in alkane and alkane derivatives in bulk systems²² and promotes self-assembly and long-range positional order at interfaces.²³ The second is the interaction between the subphase and the terminal end group (SE) of the organic molecule. With a much more complex nature, this interaction differs greatly from system to system according to the types of chemical groups involved and the structural properties of the substrate. The SE interaction may either oppose or promote long-range order in the monolayer, depending, for example, on its strength, on whether or not the substrate has long-range order (i.e., is crystalline or not), and if it has long-range order, on whether or not the order favored by the substrate-generated spatial modulation of the binding energy—the so called corrugation potential—is commensurate with that favored by the IC interaction.

Even when constructed from molecules with the same chemical backbones, the structures and properties of SAMs and LAMs may be vastly different. This reflects a different balance of the two interactions discussed above, as well as significant differences in the substrate properties. For SAMs, the SE binding energy greatly exceeds the IC interaction. For example, for thiols on gold the covalent Au-S bond strength is²⁴ ~ 400 kJ/mol, as compared to²⁵ ≤ 1 kJ/mol for the van der Waals IC interaction per a single CH₂ unit of the alkyl chains. By contrast, for LAMs on water the SE-hydrogen bond strength is²⁵ ≤ 10 kJ/mol, which is comparable to or less than the IC interaction for alkyl chains 10–20 carbons long. Even the corrugation potential of SAM substrates, of order 10–20% of the SE energy,^{20,26} is still considerably larger than the full SE-hydrogen bond strength in LAMs. Furthermore, the SAM substrate is usually a crystalline solid with a rigid, long-range ordered lattice. Dependent on substrate and temperature, commensurate, uniaxial-incommensurate, or two-dimensionally incommensurate SAM structures have been observed, with the former two reflecting the strong influence of the substrate on the SAM's order. SAMs are almost always densely packed, and once formed, their areal density cannot be changed by a lateral pressure. By contrast, LAM substrates are liquid and possess no long-range order and hence no corrugation potential. The order encountered in LAMs is therefore clearly not induced epitaxially. Furthermore, the subphase molecules are free to move laterally to accommodate the structure favored by the chains. This allows induction of reversible structural variation in the LAMs, from an expanded to a dense packing, by applying a lateral surface pressure.

Alkanethiol films on mercury cannot be classified as either SAMs or LAMs. For example, the Hg-S binding energy, ~ 200 kJ/mol,²⁴ is much larger than the IC interaction in SAMs. This energy is comparable to the SE interaction of thiols on solid Au, Ag (~ 200 kJ/mol²⁴) and Cu (~ 280 kJ/mol²⁴)—and twentyfold stronger than the ~ 10 kJ/mol hydrogen bond of LAMs.²⁵ On the other hand, in common with LAMs, the substrate is liquid; its surface lacks an intrinsic long-

range order that can be imposed on the monolayer, and the surface atoms are free to move laterally to accommodate ordering in the monolayer. The system of thiols on Hg is, therefore, an intermediate system that can be used to disentangle the influence of the SE bond strength from the lattice periodicity as reflected in the corrugation potential. Moreover, several methods (discussed below) can be employed to tune the relevant interactions in our system, bringing it close to either one of the two extremes. This allows, in principle, the possibility of studying the structural implications of variations in the relevant interactions over a wide range of conditions and, eventually, to control the layer's structure at the molecular level.

A large body of thermodynamic and other macroscopic data is available in the literature for organic monolayers on liquid mercury, both at the gas²⁷ and electrochemical interfaces.^{28,29} In some of these, indirect evidence—such as the limiting area per molecule—is used to postulate a molecular structure for the monolayer, which is significantly different than that of LAMs of the same molecules on water. For example, ring compounds tend to lie flat on water, but are expected to stand on edge on Hg, whereas alkyl compounds at low surface coverage are expected to lie flat on Hg, but would be standing up on water.²⁷ These, and other postulated effects, have not been tested by direct structural methods.

At the aqueous or electrolyte interface, the properties of the thiol-coated Hg surface have been investigated by measuring the current voltage characteristics.³⁰⁻³² Demoz and Harrison have shown that a hexadecanethiol monolayer on the mercury surface forms an insulating film where the current is reduced by as much as 20,000 when compared to the bare electrode.³⁰ This implies that a defect-free, uniform thiol film covers the surface. Bruckner-Lea and coworkers have extended these measurements by controlling the surface area of the thiol-coated mercury electrode.³² Their studies show that an expansion of the surface area produces defects and pinholes in the thiol film that are almost completely removed when the drop is compressed back to its initial surface area. However, neither of these studies provides direct structural information on the thiol surface layer.

Structural studies of thin organic films on liquid metal surfaces have received practically no attention compared with studies on solid supports. Liquid metal surfaces present unique characterization problems since UHV electron-diffraction techniques are hampered by the high vapor pressure of the mercury and the samples cannot be easily manipulated. Scanning tip techniques are also unsuited for studies of liquid metal surfaces since the tip interaction disturbs the nature of the liquid surface. Furthermore, the rastering times of these techniques are too long, as compared with the atomic motions, to obtain "snapshots" of the

atomic packing at the surface. Despite these problems (unsuccessful) attempts have been made to image the thiol-coated Hg surface using STM.³³

Surface X-ray scattering techniques are emerging as a direct probe of the structure of liquid metal surfaces, as evidenced by recent studies of the surfaces of liquid mercury^{34,35} and liquid gallium.³⁶ These reflectivity studies have also been extended to binary alloys^{37,38} and oxides on liquid metal surfaces.³⁹ For clean Hg and Ga surfaces, broad peaks in the X-ray reflectivity spectrum are found, clearly proving the long-predicted atomic layering near the surface and showing a decay length of the layering of a few atomic diameters. Grazing-incidence diffraction shows that the in-plane structure near the surface is liquid-like, in spite of the layering order normal to the surface.³⁵ The surface roughness of mercury was found in these studies to be $\sigma \approx 1.1 - 1.4 \text{ \AA}$, in excellent agreement with capillary wave theory.⁴⁰ Although the microscopic roughness for single-crystal substrates is also sub- \AA over a single crystalline facet, these facets, which are hundreds to thousands of \AA on a side, are separated from each other by single or multiple atomic steps, which, of course, do not exist at the liquid surface. Thus, the ultra-smooth liquid metal surfaces—which, unlike solid crystalline surfaces, are free from any static structural surface features like atomic steps and defects—are deemed to be almost ideal substrates for organic films.

Apart from our measurements on alkanethiols on mercury, only two other X-ray experiments of organics on a liquid metal have been published. The first, a study of stearic-acid-covered Hg,⁴¹ used grazing-incidence diffraction exclusively and addressed only the question of the adsorbate's possible influence on the structure of the liquid surface. Two grazing-incidence diffraction peaks, interpreted as indicating a hexagonal packing in the monolayer, were resolved. In the absence of reflectivity measurements, however, the structure of the layer normal to the surface could not be determined, nor could proof be provided that the observed peaks originated in a monolayer rather than a multilayer or even small three-dimensional crystalline particles. Very recently, Harzallah and coworkers⁴² employed X-ray reflectivity to show that well-defined monolayers of several fatty acids with molecules oriented normal to the surface could be prepared on the surface of mercury. No attempt was made in that study to determine the in-plane structure of the monolayers by grazing-incidence diffraction.

Using synchrotron X-ray reflectivity and grazing-incidence diffraction, we have studied the structure of thiol films on the surface of mercury.⁴³ The monolayers were found to be very uniform, with densely packed molecules well aligned along the surface normal. Yet, contrary to expectations and in marked contrast to both SAMs and LAMs, grazing-incidence diffraction revealed no sharp in-plane peaks, indicating that no long-range lateral order is established

within the monolayer. This was attributed to the strong epitaxy of the layer to the disordered liquid substrate. The liquid-like in-plane structure and layering along the surface normal, which are observed for the bare liquid surface, are maintained also when covered by the organic film. For higher dosages of thiols, multilayers are formed. In contrast to the monolayers, more than 10 sharp grazing-incidence diffraction peaks were found, indicating that the multilayers are highly ordered in-plane. The crystallographic structure of the film was determined both in-plane and normal to the surface. The implications of these results to LAM and SAM structures are discussed below in detail, as are ways of extending these measurements to provide more comprehensive answers to the issues raised above.

6.2 Experimental

Detailed discussions of techniques and procedures for X-ray diffraction and reflectivity measurements of organic monolayers on liquid surfaces are available in the literature¹⁰ and will be discussed here only briefly. We will, however, discuss in some detail the special features peculiar to measurements on liquid metal surfaces.

6.2.1 SAMPLES AND SAMPLE CELL

A sketch of the sample cell used in most of the measurements is shown in Fig. 1a. It consists of a sealed glass vessel with panoramic Be X-ray windows (D) allowing X-ray access over the required angular range. A glass trough (A) residing at the bottom of the cell is filled with liquid Hg from a sealed reservoir (B) through a glass capillary (C). The cell and reservoir are kept under an oxidation-preventing hydrogen gas atmosphere, introduced via the gas handling system (E). Earlier measurements performed in a nonsealed cell gave similar results but were not as stable in time as those presented here. The cell is mounted on an active vibration isolation table (F), which virtually eliminates all vibrational pickup by the rather thick (3–4 mm) mercury pool. The isolation table is mounted, in turn, on the liquid surface reflectometer.

In our study we investigated alkanethiols, $\text{CH}_3(\text{CH}_2)_{n-1}\text{SH}$ (denoted C_n in the following) with $n = 8, 12, 16, 18, 22, 30$. Monolayers were deposited on clean liquid Hg surfaces by various techniques: direct application of the thiols in their liquid state, chemical vapor deposition, self-assembly from an ethanol bath as per the standard practice for SAMs, and spreading from a dilute chloroform solution as per the standard practice for LAMs on water. Multilayers were formed by

either extended vapor deposition or direct application of the thiols. We found that, regardless of the deposition technique, well-defined layers could be obtained reproducibly, showing identical X-ray characteristics. Furthermore, the films were stable over the several hours required to take the X-ray measurements. Precautions like keeping the incident X-ray flux as low as practical, using an oxygen-free environment, etc., were taken to keep beam damage effects to a minimum. All experiments were performed at room temperature.

6.2.2 SURFACE X-RAY MEASURING TECHNIQUES

The structure of the films was investigated by grazing-incidence X-ray diffraction (GIXD)—a technique sensitive to the atomic and molecular structure within the surface plane—and X-ray reflectivity (XR), which probes the surface-normal electronic density profile. Detailed accounts of both are available in the literature,¹⁰ and therefore will be discussed here only briefly. The experimental geometry is shown in Fig. 1b. The XR is obtained with $\alpha = \beta$ and $2\theta = 0^\circ$, while GIXD is obtained for $\alpha < \alpha_c$ and $2\theta \neq 0^\circ$, where α_c is the critical angle for total external reflection.

The XR measurements over the range $0 \leq q_z \leq 2.5 \text{ \AA}^{-1}$, where $q_z = (4\pi/\lambda) \sin \alpha$, were done at beamline X22B and the wiggler beamline X25 at the NSLS. The absolute reflectivity was obtained from measurements along the specular axis ($2\theta = 0^\circ$), subtracted by the diffuse background measured at $2\theta = \pm 0.6^\circ$, and normalized by the direct beam intensity. The GIXD measurements were done at the TROIKA undulator beamline at the ESRF and remeasured (with identical results) at beamlines X22B and X25 at NSLS employing wavelengths in the range $0.65 \text{ \AA} \leq \lambda \leq 1.2 \text{ \AA}$. The incidence angle for the GIXD measurements was $\alpha = 0.2^\circ = 0.6\alpha_c$, and the vertical acceptance of the detector was $0 \leq q_z \leq 1.1 \text{ \AA}^{-1}$. The in-plane momentum transfer is given by $q_{\parallel} = (4\pi/\lambda) \sin \theta$.

6.2.3 MODELING AND FITTING

The measured XR data, $R(q_z)$, can be modeled using the relation

$$R(q_z)/R_f(q_z) \approx | (1/\rho_\infty) \int dz [\partial \langle \rho(z) \rangle / \partial z] e^{iq_z z} |^2$$

valid within the Born approximation, i.e., for $\alpha \geq 4\alpha_c$ or $q_z \geq 0.2 \text{ \AA}^{-1}$ in our measurements. Here $\langle \rho(z) \rangle$ is the electron density at depth z averaged over an area of the surface that corresponds to the X-ray resolution, ρ_∞ is the bulk electron density, and R_f is the Fresnel reflectivity for an ideally smooth and

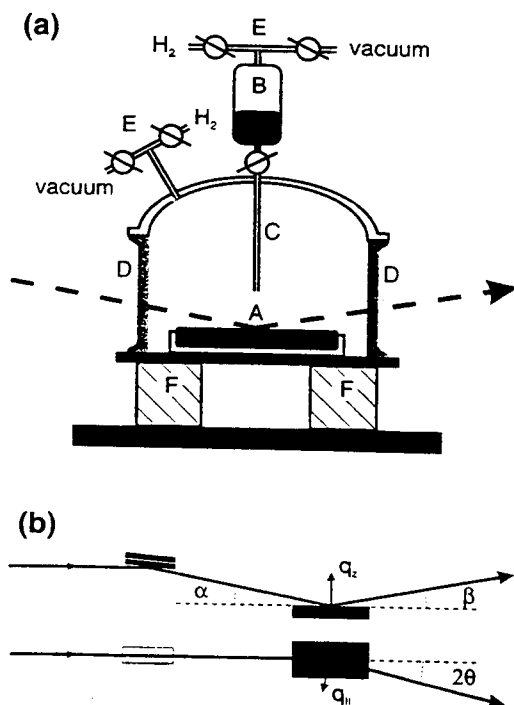


FIG. 1. (a) Schematic drawing of the cell used for the X-ray surface diffraction measurements on liquid Hg, showing the trough containing the liquid Hg sample (A), the Hg reservoir (B), the capillary sample inlet (C), the X-ray windows (D), the gas handling manifold (E), the active vibration isolation table (F), and the X-ray beam (dashed line). (b) Side (upper) and top (lower) views of the diffraction geometry. The incident beam is tilted down to impinge on the liquid surface at an angle α by a Ge single crystal. The detector measures the intensity of an X-ray diffracted vertically at an angle β relative to the surface and a horizontal angle 2θ relative to the specular reflection plane. q_z and $q_{||}$ denote the surface-normal and in-plane components of the scattering vector.

abrupt interface.^{44,10} Typically, a physically motivated model is constructed for the density profile $\langle\rho(z)\rangle$, inserted into the equation above which is then calculated analytically and fitted to the measured reflectivity data to extract the parameter values that best describe the profile. In the case of a bare mercury surface, the oscillatory density profile $\langle\rho(z)\rangle$ was modeled by a number of Gaussians whose width increases with the distance of each Gaussian from the surface, such that the density becomes uniform when the widths exceed the distance between adjacent Gaussians. The structure was also broadened by convolution with the atomic scattering factor.³⁴

For the thiol-covered Hg surface, we modified this model profile by adding on top n Gaussians, each of which represents a CH_2 group of the alkyl chain and

an additional Gaussian representing the terminal sulfur. The model for the multilayer data was constructed in an analogous way. The carbon-carbon and the carbon-sulfur spacings along the surface normal were fixed at 1.27 Å and 1.5 Å, respectively. These spacings correspond to the projections of the carbon-carbon (1.53 Å) and the carbon-sulfur (1.82 Å) bonds onto the molecular axis. The in-plane area per molecule was fixed at that of the multilayer phases (19.23 Å²), as measured by GIXD.

6.3 Results

In this section we describe the XR and GIXD results obtained for monolayer and multilayer thiol films and their modeling in some detail.

6.3.1 MONOLAYERS

Reflectivity

The measured X-ray reflectivities $R(q_z)$ of the bare liquid Hg as well as surfaces covered by C₈, C₁₂, C₁₆, and C₁₈ are shown in Fig. 2. Note first that both the bare (R_{Hg} , dashed line) and the thiol-covered (R_{C_n} , open circles) reflectivities are only a little lower than the Fresnel reflectivity (R_f , solid line) of an ideally flat surface. This indicates a similar, small surface roughness for the bare and thiol-covered Hg surfaces. Although R_{C_n} dips significantly below R_{Hg} for $q_z > 0.5 \text{ \AA}^{-1}$, they approach each other again at the broad peak around 2.15 \AA^{-1} . Since this peak characterizes the atomic surface layering of the Hg subphase,³⁴ its persistence here for the thiol-covered surface indicates that adsorption of the organic molecules causes no major changes in the liquid metal surface structure. A similar conclusion was obtained for fatty acid layers on Hg by Barton et al.⁴¹ and Harzallah et al.,⁴² although the SE interactions in both of these studies are much weaker than here. The most significant change, compared with the bare mercury surface, is the emergence of periodic oscillations, which result from interference of waves reflected from the thiol/air and thiol/mercury interfaces. The oscillations are highlighted by normalizing the measured R_{C_n} curves by the Fresnel reflectivity R_f . The resulting R/R_f curves are presented for C₁₂ and C₁₈ in Fig. 3. For the R_{C_n} curves shown, four to five equally spaced oscillations are observed, which is considerably more than that achievable for equal-thickness LAMs on water, where the low surface tension—and consequent higher roughness from capillary wave fluctuations—limit the measurable q_z range to $\leq 0.6 - 0.7 \text{ \AA}^{-1}$. Consequently, the spatial resolution achievable for LAMs on water is correspondingly lower. The period Δq_z of the fringes, marked on the

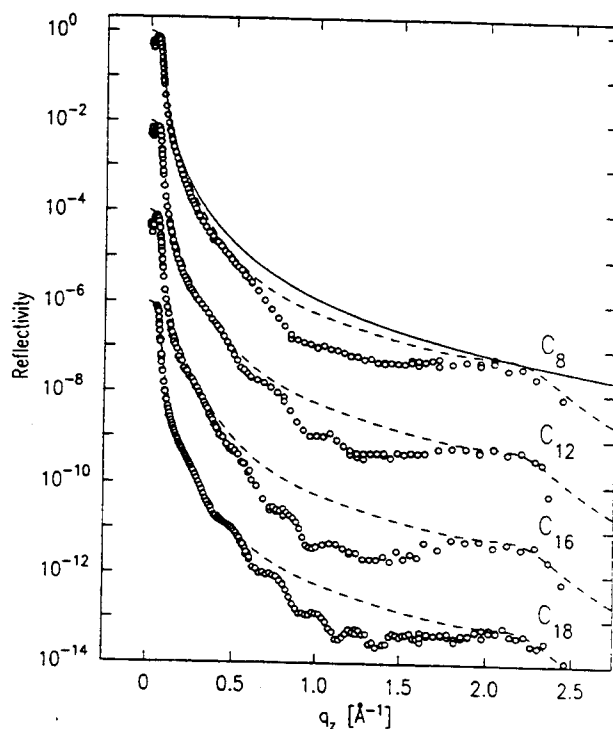


FIG. 2. X-ray reflectivities of bare (dashed line) and C_8 , C_{12} , C_{16} , and C_{18} monolayer covered liquid Hg surface. The curves are shifted relative to each other by two decades for clarity. The Fresnel reflectivity R_f (solid line) is also shown. The presence of the monolayer is clearly indicated by the periodic modulations of the curves, the so-called Kiessig fringes.

figure, correspond to a layer thickness of $d = 2\pi/\Delta q_z = 17.5 \text{ \AA}$ and 25 \AA for C_{12} and C_{18} , respectively. These values are in excellent agreement with the length of the fully extended C_n molecules, $(n-1) \times 1.27 + 1.50 + 2.2 \text{ \AA}$, where 1.27 \AA , 1.50 \AA and 2.2 \AA are the surface-normal projected lengths of the $\text{CH}_2\text{-CH}_2$, $\text{CH}_2\text{-S}$, and S-Hg bonds, respectively, derived from bulk thiolates.⁴⁵ The overall shapes and features of the reflectivities for all chain lengths studied are the same, except, of course, for the periods of the oscillations. However, for long chains ($n = 22, 30$) the fringes are weak, which indicates high interfacial roughness and less well-defined layers.

The model discussed in the previous section was fitted to the measured reflectivities, using identical parameters for all data sets (apart from the number of CH_2 groups). As the solid lines in Fig. 3 show, the results are in excellent agreement with the experimental data. The density profiles (normalized to the bulk Hg electron density), corresponding to the fits shown in Fig. 3, are plotted in

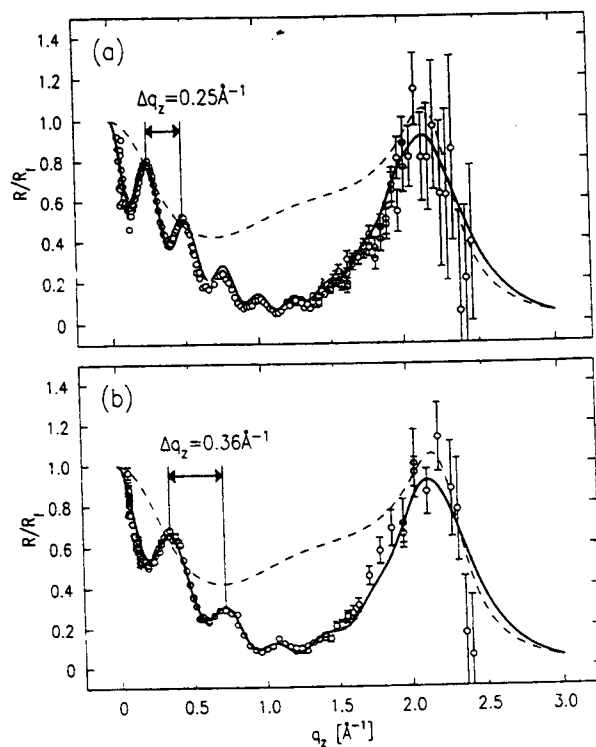


FIG. 3. The measured normalized reflectivities R/R_0 of (a) C_{18} and (b) C_{12} monolayers on liquid Hg (circles) and of the bare Hg surface³⁴ (dashed line). The different periodicities Δq_z for C_{18} and C_{12} are indicated. Solid lines are fits to the model described in the text with the fit parameters differing only in the number of CH_2 groups. (Reprinted with permission from Nature 384, 250 (1996). Copyright 1996 Macmillan Magazines Ltd.)

Fig. 4. Comparison with the density profile of the clean Hg surface (dashed line) reveals the extended hydrocarbon tail, the higher-density sulfur atom in between the Hg and hydrocarbon tail, and a slight decrease in the amplitudes of the first Hg layers. This decrease upon coverage with thiols likely reflects the small increase in surface roughness expected from the capillary wave theory⁴⁰ due to a small decrease in the surface tension. Nevertheless, the layered structure of the Hg interface, its decay length, and other properties remain unchanged upon coverage of the surface by thiols despite the strong S–Hg covalent bond. Furthermore, the surface roughness (estimated from the density profile width of the first Hg layer) remains about 1 \AA , which is in good agreement with the value given by capillary wave theory.³⁴ This confirms the uniqueness of liquid metal surfaces as atomically flat substrates of macroscopically large lateral dimensions.

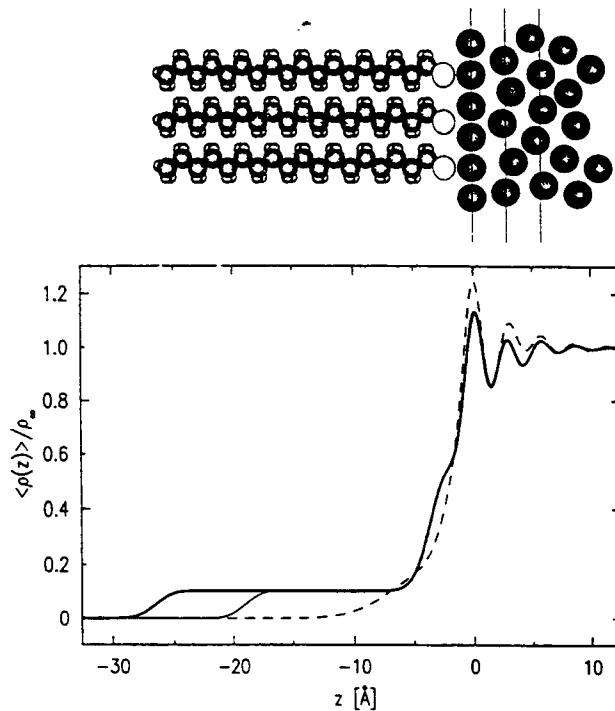


FIG. 4. Schematic drawing (upper) of the molecular stacking and (lower) normalized electron density profiles $\langle \rho(z) \rangle / \rho_{\infty}$ (with Hg bulk electron density ρ_{∞}) obtained from the fits of the model for C_{18} (bold line) and CH_{12} (thin line). The upper and lower figures are aligned with each other. Vertical lines in the model mark the positions of the three outermost Hg surface layers, with the origin of z coinciding with the first Hg layer. Since the Gaussian width describing the CH_2 groups (typically $\sim 1.2 \text{ \AA}$) is considerably greater than half the separation between the carbon atoms, the density profile appears constant in the central part of the chain. (Reprinted with permission from Nature 384, 250 (1996). Copyright 1996 Macmillan Magazines Ltd.)

As discussed below, GIXD measurements yield an accurate value of 19.23 \AA^2 for the area/molecule of the thiol multilayers. All model fits to the monolayers discussed so far employed this value as a fixed parameter. The good fits and the closeness of the resultant layer thickness to the extended molecule's length in all cases strongly support the conclusion that this molecular area is indeed correct for monolayers as well. When allowed to vary in the fit, the area/molecule in the monolayer fits converges to a slightly lower value of 18.75 \AA^2 , which is, nevertheless, still close to the multilayer value. Regardless of this small uncertainty, the agreement between the two sets of values—those refined from the XR measurements and those obtained from the GIXD (of multilayers)—

indicate that the coverage of the surface by the layer is complete to within a few percent at most and that its density is very high; it is comparable to those of crystalline monolayers formed by surface freezing on alkane and alcohol melts²³ and fully compressed LAMs on water.¹²

GIXD

Both the high density found in the XR measurements for the adsorbed thiol layer and the extended molecular conformation indicated by the measured layer thickness require a close packing of the molecules. Therefore, one may expect that the layer will show in-plane long-range ordering of the molecules. Nevertheless, exhaustive GIXD measurements at two of the most intense beamlines worldwide, X25 at the NSLS and TROIKA at the ESRF, failed to show any in-plane peaks for the monolayer phases of thiol molecules of any of the examined lengths. Observation of such peaks would have indicated the existence of an ordered adlayer structure. In particular, a careful search was done from 1.5 to 1.7 Å⁻¹, where structurally similar SAMs and LAMs (as well as our multilayer measurements) show the lowest-order in-plane peaks. In Fig. 5 we show the measured GIXD data for the C₁₈ thiol monolayer (solid line) and for the clean Hg surface (dash line). Both show the characteristic broad peaks around the in-plane wavevectors $q_{\parallel} \approx 2.3 \text{ \AA}^{-1}$ and $q_{\parallel} \approx 4.5 \text{ \AA}^{-1}$ expected for liquid mercury³⁵ (although at different relative intensities, which may indicate a very slight thiol-induced modification of the in-plane structure of the Hg surface). As we discuss below, the absence of in-plane order in the densely packed alkanethiol monolayer is most likely promoted by the disordered Hg subphase via the strong, covalent Hg-S bond.

It is worth noting that the same reflectivity and in-plane results described above were obtained also in measurements of thiol-covered Hg in air. By contrast, for the bare (i.e., not covered by thiols) Hg surface in air, high surface roughness and pronounced mercury oxide diffraction peaks are observed. This indicates that the thiol monolayer acts as a barrier that protects the surface from oxidation, as it does also on solid metal surfaces.⁴⁶ This, as well as electrochemical charge transfer experiments,³⁰⁻³² strongly support our results of the close packing of the thiol monolayer.

In Fig. 6 we summarize the structure of the thiol monolayer on mercury as it emerged from the results described above: an underlying layered mercury subphase and a sulphur-bound monolayer of vertically aligned, densely packed, yet in-plane disordered, thiol molecules. The implications of this packing on the roles played by the various interactions in the determination of the monolayer's structure are discussed in the next section.

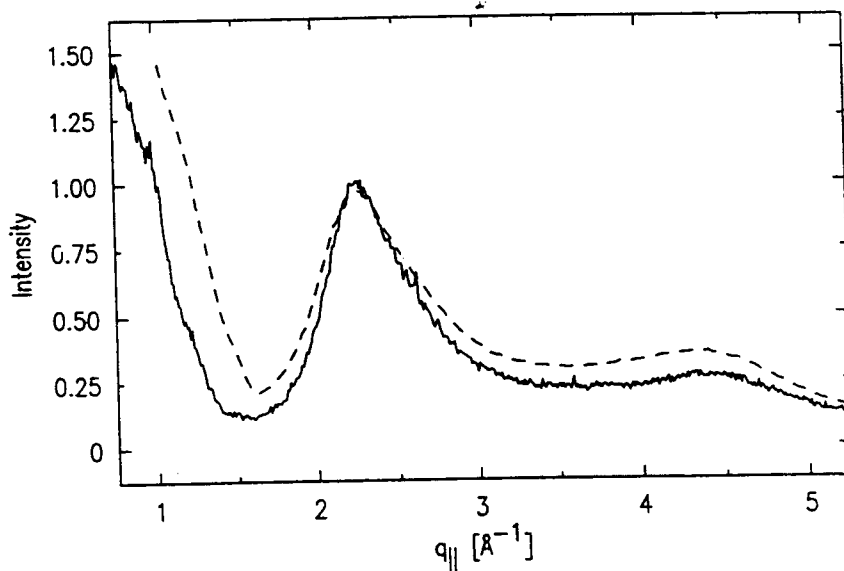


FIG. 5. GIXD patterns of a bare (dashed line) and a C_{18} -monolayer-covered (solid line) Hg surface, measured with an incidence angle $\alpha = 0.2^\circ = 0.6\alpha_c$ and a vertical detector acceptance of $0 \leq q_z \leq 1.1 \text{ \AA}^{-1}$. Only the broad peaks corresponding to the Hg liquid structure factor are found in the monolayer data (in-plane resolution $\Delta(2\theta) = 5 \text{ mrad}$). The absence of sharp diffraction peaks from the thiol monolayer indicates that no long-range in-plane order is established in this layer, in spite of its dense packing. (Reprinted with permission from *Nature* 384, 250 (1996). Copyright 1996 Macmillan Magazines Ltd.)

6.3.2 MULTILAYERS

Reflectivity

At higher thiol coverages, distinct changes in the reflectivity curves are observed, indicating the formation of multilayer structures. As will be shown below, these multilayers correspond to the epitaxial growth of mercury thiolates. A typical reflectivity curve for a C_{12} thiol multilayer on mercury is shown in Fig. 7. The curve exhibits peaks with a period $\Delta q_z \approx 0.175 \text{ \AA}^{-1}$, which is close to half that of the corresponding period for a monolayer (Fig. 3). This indicates a multilayer structure with a repeat distance along the surface normal $d = 2\pi/\Delta q_z = 35.9 \text{ \AA}$, which is close to that of two fully extended thiol molecules (i.e., bilayer stacking). Several features of the raw data stand out immediately. Since the reflectivity follows that of the bare liquid Hg, the surface roughness of the multilayers remains low: $\sim 1 \text{ \AA}$. Also, the layering peak at

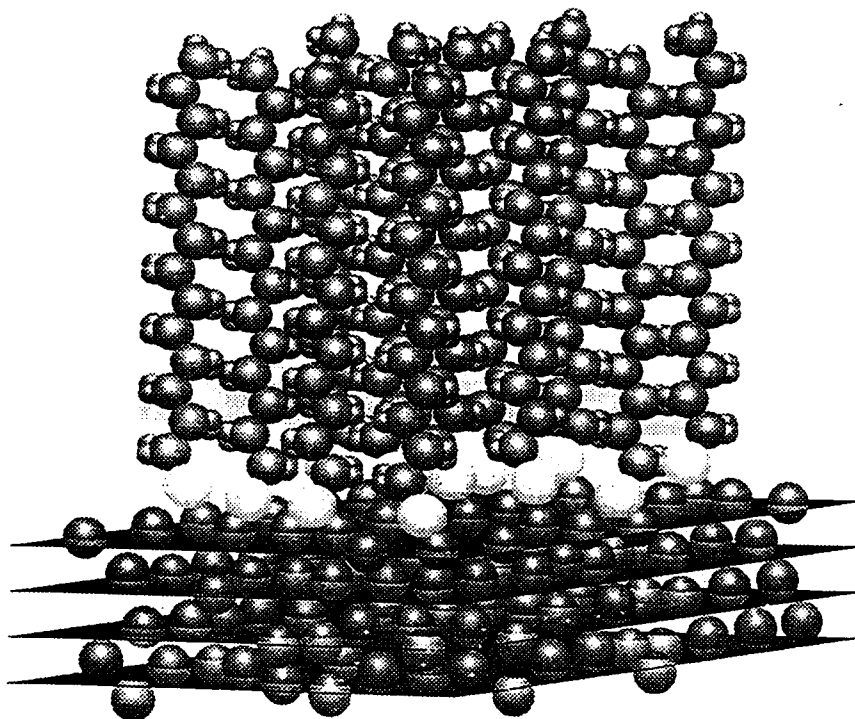


FIG. 6. Model of the alkanethiol monolayer on the liquid Hg surface. The laterally disordered long alkythiol molecules are oriented along the surface normal and bind with their terminal sulfur atoms to the topmost Hg layer. The layering of the Hg atoms in the near-surface region is highlighted by the parallel planes. (Reprinted with permission from Nature 384, 250 (1996). Copyright 1996 Macmillan Magazines Ltd.)

$q_z = 2.2 \text{ \AA}^{-1}$ seems to persist in all X-ray reflectivity patterns, indicating that the multilayer does not disturb significantly the layering effect at the surface of the mercury subphase. The greater intensity of the even-indexed peaks relative to those of the neighboring odd-indexed peaks in the reflectivity modulations results from differences in the "monolayer" and "bilayer" structure factors. The appearance of sinusoidal modulations, rather than sharp Bragg peaks, indicates that there are only a few bilayers present, possibly just one or two. In addition, the absence of Kiessig fringes, especially at small q_z , indicates either the presence of a single bilayer or a variation in the number of bilayers during the measurement time and/or across the X-ray illuminated area of the surface. The high modulation amplitude observed, more than tenfold that observed for monolayers, requires high electron density variations along the surface normal of the bilayer. The most

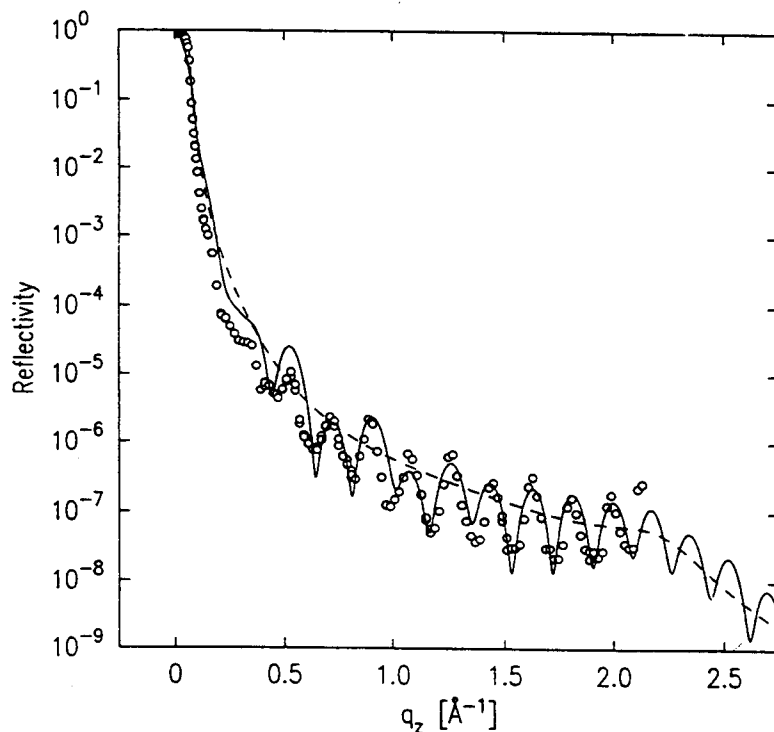


FIG. 7. X-ray reflectivity of a C_{12} thiol multilayer on liquid Hg (circles). The reflectivity of the bare Hg surface (dashed line) and a fit to the experimental data (solid line) are also shown. The fit indicates the existence of one bilayer of mercury thiolate residing on top of the single-monolayer-covered mercury surface, as described in Fig. 8.

probable source for such a high electron density is the intercalation of Hg atoms into the bilayer. A similar structure has recently been reported for bulk Hg thiolates, albeit with very short chain lengths, where planes of Hg atoms are separated by thiol bilayers with the binding sulfur atoms above and below the Hg planes.⁴⁵

To obtain a more quantitative description of the multilayer's structure, a model was constructed for the density profile using the same general approach of the monolayer model presented above. Here a variable number of bilayers are added on top of the thiol-monolayer-terminated Hg surface where in each bilayer there is one Hg atom sandwiched between the sulfur head groups of the two thiol molecules (as shown in Fig 8). The area of the in-plane two-dimensional unit cell was fixed at 19.23 \AA^2 , determined from the GIXD measurements (see below), and the surface-normal d-spacing of the bilayers was allowed to vary in the fit. The

best fit to a model composed of a single bilayer on top of the monolayer is shown in Fig. 7 as a solid line, and the corresponding electron density profile is given in Fig. 8. Here the bilayer thickness is found to be 34.1 Å, which is very close to twice the monolayer thickness (17.5 Å). Models assuming either two or three bilayers result in similar quality fits, with almost identical bilayer thickness. Hence, although the reasonable fit verifies the general features of the model proposed, the details should be regarded as tentative only. The generally lower fit quality for multilayers (as compared to the monolayer fits) may result from possible local and/or temporal variations in the number of bilayers over the area illuminated by the X-ray beam and/or other structural imperfections in the multilayer. Also, a more sophisticated model that would take into account different structural motifs may be required to fully describe the complex structure of the multilayers. Further work on this is clearly necessary.

To further verify that the multilayers are indeed structurally similar to thiolates—rather than being a pure, Hg-free, alkanethiol phase—the structure of *bulk* Hg thiolates prepared as powder by reacting C_{12} and C_{18} alkanethiols with mercury acetate was investigated using high-resolution powder diffraction at

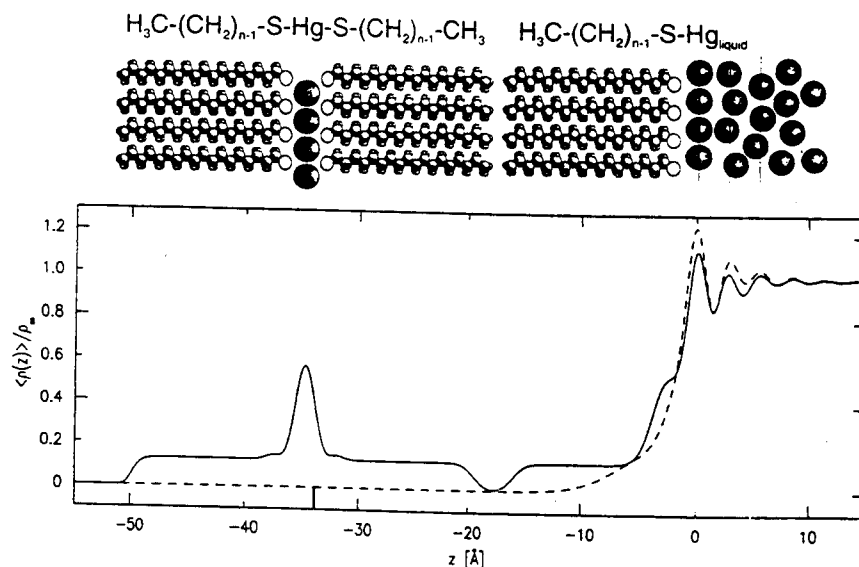


FIG. 8. (Upper) A schematic model of the layer stacking in the C_{12} thiol multilayer, obtained from the fit to the measured data in Fig. 7. (Lower) The corresponding density profile. The layer consists of a single thiol bilayer sandwich (of internal structure thiol-Hg-thiol) adsorbed on top of the thiol-monolayer-terminated Hg surface. Note the high-density Hg monolayer intercalated in between the two thiol monolayers and attached at both sides to the sulphur of each thiol, represented by the intermediate density layers on both sides of the mercury layer.

beamline X7A of the NSLS. The resultant spectrum includes diffraction peaks, which are in good agreement with the peaks observed for the multilayers. For example, the low- q peaks of the C_{12} mercury thiolate powder are observed at $q(00l) = l \times 0.1801 \text{ \AA}^{-1}$, yielding a c -axis layer spacing $d = 2\pi/\Delta q_z = 34.89 \text{ \AA}$; this is very close to that of the bilayer. A full structural analysis of the complex monoclinic structure of the thiolates was not attempted.

Neither the formation process of these multilayers nor the parameters controlling it are well understood yet, and reproducible production of multilayers of a given number of layers is still much of an art. We also note that multilayer phases form more easily for the shorter, higher-vapor-pressure thiols; for $n \geq 18$ no multilayers could be observed. Perfecting a procedure for producing these multilayers and easily controlling the number of bilayers is a prerequisite for further advance in the detailed study of their structure and the possible dependence of the structure on the number of layers.

GIXD

In marked contrast to the GIXD measurements on monolayers where no diffraction peaks were observed, for multilayers we found sharp, well-separated diffraction peaks. In Fig. 9 we show the pattern measured for C_{12} (thin solid line). It includes over ten diffraction peaks that can be indexed by an oblique unit cell with lattice parameters $|a| = 4.31 \text{ \AA}$, $|b| = 4.72 \text{ \AA}$, $\gamma = 71^\circ$, as shown in the inset. The calculated diffraction peak positions for this structure are marked by vertical arrows at the bottom of the figure and are in excellent agreement with the positions of the observed lines. The area occupied by each molecule in this structure is 19.23 \AA^2 , a value used in the XR fits and corroborated by those results (as discussed above). The resolution-limited width of the peaks indicates that the in-plane order is long-range and extends over a resolution-limited coherence length of at least 1000 \AA . A full structural refinement, including the intensities, will have to await a measurement with higher statistical accuracy.

The diffraction patterns obtained from the GIXD for different chain lengths are similar in their peak positions and intensities. The three lowest-order peaks of the patterns obtained are for C_8 at 1.42, 1.54, and 1.71 \AA^{-1} , for C_{12} at 1.41, 1.54, and 1.71 \AA^{-1} and for C_{16} at 1.46, 1.57, and 1.70 \AA^{-1} . The similar positions indicate that the in-plane crystallographic structure of the multilayers is to a large extent length independent. The smaller q_{\parallel} values, and correspondingly larger in-plane repeat distances, observed for C_{16} may be indicative of a small tilt of the molecules from the surface normal. Tilts of $5\text{--}10^\circ$ cannot be extracted from the very complex reflectivity curves of the multilayers, such as that shown in Fig. 7.

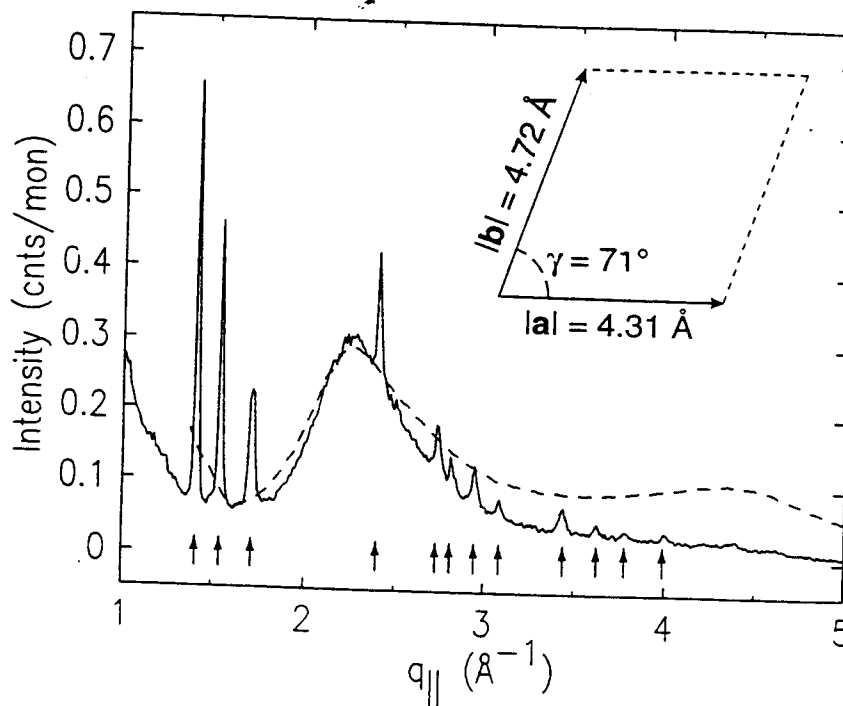


FIG. 9. Grazing-incidence diffraction patterns of a bare (dashed line) and a C_{12} multilayer-covered (solid line) Hg surface (experimental parameters are the same as in Fig. 7). At least 12 sharp, resolution-limited diffraction peaks are visible in the pattern measured for the multilayer, indicating a well-ordered in-plane structure. The calculated unit cell is displayed in the upper right side of the figure. The calculated peak positions corresponding to this cell are marked by arrows at the bottom of the figure and are in excellent agreement with the observed diffraction pattern.

On the basis of the present data, we also cannot ascertain the registry between adjacent thiol layers or between the thiol and intercalated Hg layers.

6.4 Discussion

The results obtained in these measurements highlight the role of organic films on liquid metals as an intermediate case between Langmuir films on water (or organic liquids) and self-assembled monolayers on crystalline substrates. The monolayer data illustrates the importance of the relative strengths of the SE and IC interactions and the specific order preferred by each. The observation of sharp GIXD peaks in monolayer systems dominated by IC interactions—like the densely packed phases of LAMs of alkanes, alcohols, and fatty acids on pure

water¹²—demonstrate that long-range in-plane order is usually established in such systems.

Although the confinement of the film to the surface in LAMs on water by the hydrophobic interactions of the chains with the subphase may have a stabilizing effect on these LAMs, it is by no means a necessary condition for establishing order in the surface layer. This is demonstrated by a series of measurements at the free surface of single-component bulk melts of alkanes and of alcohols,²³ where crystalline mono- or bilayers were observed on the surface of the bulk melt at temperatures up to a few degrees above the bulk freezing point. In these cases the "monolayer" and "subphase" molecules are identical, and of course fully miscible so that the monolayer molecules are not confined to the surface. However, both systems are dominated by the IC interactions, and the SE bonds (~ 10 kJ/mol hydrogen bonds in the case of LAMs on water and ~ 1 kJ/mol van der Waals in the case of alkanes and alcohols on their own melts) are weaker than those of the IC interactions for chains of lengths $n \geq 10 - 15$ carbons. The conclusion is, therefore, that the IC interactions are responsible for the long-range order in these systems. For Langmuir monolayers, with only a few exceptions the SE interactions with the disordered atoms of the liquid subphase are too weak to cause more than slight changes in the structure relative to that favored by the IC interactions in these films.

The spatial variation of the SE interaction parallel to the surface—the so-called corrugation potential—may either promote or oppose the ordering favored by the IC interactions, depending on the match between the packing arrangement and periodicities favored by these two interactions. For example, for thiol SAMs on crystalline Au surfaces⁴⁷⁻⁴⁹ the corrugation potential tends to favor well-ordered monolayers that may be either commensurate or uniaxial-incommensurate with the underlying metal. Here the mismatch between the two structures is small, and the small difference between the underlying substrate and alkane spacings is compensated for by a molecular tilt in the SAM. The enhanced stability of the SAM, resulting from the strong SE interaction, is reflected in the elevated melting temperature of alkane thiols on Au(111) as compared to that of the bulk.⁴⁷

Although the strength of the SE interaction of thiols on Hg (~ 200 kJ/mol) is similar to that of thiols on crystalline Au, Cu, and Ag, the liquid Hg surface has no intrinsic long-range order, i.e., no underlying corrugation potential to impose its order on the thiol monolayer. It could be expected, therefore, that the absence of interference from the substrate's ordering field will promote the formation of order in the film by the IC interactions, as occurs in LAMs. Furthermore, the Hg atoms of the liquid substrate, although strongly bound to the thiol molecules, are free to move laterally to accommodate the order preferred by the IC interactions. However, reversing this argument implies that any order induced by the IC interaction is highly likely to be imposed on the surface Hg atoms as well be due

to the same very strong SE interaction. Assuming the layer to have the same structure as found for alkanethiols on Au and Ag, this would require a 5–10% compression of the Hg atoms in the surface layer. This compression would carry a great energy cost. In addition, the consequent order induced in the Hg surface layer, at a temperature where the bulk is disordered, would represent a large increase in the entropic contribution to the Hg surface free energy. For these two reasons, the induction of order in the Hg surface layer by the thiol monolayer appears highly unlikely. We conclude therefore that the opposite happens: The disordered liquid surface structure of the Hg subphase is imposed on the adsorbate film, resulting in an in-plane-disordered film. A similar tendency was observed in a recent study of LAMs on water, where the strengthening of the adsorbate/liquid-subphase interaction by the addition of cosolvents inhibited the two-dimensional crystallization of the amphiphile layer.⁵⁰

While the Hg subphase suppresses the intrinsic in-plane order of the first thiol monolayer, this disordering effect does not extend beyond the first layer, thus allowing ordered multilayer phases as observed. The first thiol monolayer presents a terminal layer of methyl groups to the first bilayer that assembles on top of it. This leads to an SE interaction for the first bilayer, which is the $\text{CH}_3\text{-CH}_3$ interaction (as shown in the model in Fig. 8) discussed above. The strength of this interaction is only $\sim 1\text{--}1.5$ kJ/mol, or $\sim 1/20$ of the S–Hg bond. In addition, the ordering is promoted not only by the IC interactions between the chains but also by the strong ionic interactions between the intercalated Hg and the terminal sulfurs. Thus, with the great decrease in the SE interaction strength for the first bilayer, the total IC interactions become dominant and induce long-range order in the bilayer. This order has a similar lattice type (although highly oblique) and unit cell dimensions as is found in dense alkane and alcohol films and compressed LAMs on water, which are also IC interaction dominated.

6.5 Conclusion

The results of our studies indicate for the first time that dense, well-defined, molecular organic films on the surface of Hg can be formed, and their structure determined by precise surface-specific X-ray scattering methods. The seemingly contradictory observations of a highly developed order in the surface-normal direction (densely packed thiol monolayers and multilayers of vertically aligned molecules with a uniform thickness) and its complete absence in the in-plane direction for monolayers highlight the importance of the relative strengths of the IC and SE interactions, the corrugation potential (if any), and their preferred ordering patterns in the determination of the phase behavior of adsorbate films.

This, in turn, suggests that it may be possible to continuously tune the behavior

between the ordered and disordered in-plane regimes. First, by using different end groups the bond strength may be varied over a large range. Barrier control of the surface pressure and the concomitant variation of the area/molecule will further enhance the ordering tendencies as in conventional Langmuir films. Increasing the strength of the IC interactions by using longer, or chemically modified, chains will also increase the tendency for long-range order. In all cases, the entropic disordering effects can be reduced by lowering the temperature. Since Hg freezes at -39°C , a significant gain over water subphases is obtainable. Thus, the present results provide a new perspective into the structure of both self-assembled and Langmuir monolayers. Future studies using this system may bridge the gap between these two limiting cases, shed more light on the evolution of one into the other, and elucidate the specific roles of the various interactions in the determination of the structure of the adsorbate films.

Acknowledgments

We thank C. Chidsey for providing the C_{22} and C_{30} thiols; D. Mandler, I. Rubinstein, G. Whitesides, P. Fenter, and A. Ulman for enlightening conversations; D. Abernathy, G. Grüble, and J. F. Legrand for their collaboration in the GIXD measurements at ESRF; L. Berman for advice and assistance in the NSLS beamline X25 measurements; and D. Cox and Qing Zhu for help with the thiolate powder diffraction measurements. This work was supported by the Division of Material Sciences, U.S. Department of Energy (Grant DE-FG02-88-ER45379), the National Science Foundation (Grants DMR-94-00396 and DMR-95-23440), and the U.S.-Israel Binational Science Foundation. BNL/NSLS is supported by DOE under contract DE-AC02-98CH10886

References

1. Aristotle, *Problemata*, W. S. Hett, Trans., Book 23, no. 38, Heinemann, New York, 1937.
2. Pliny the Elder (Gaius Plinius Secundus), *Natural History*, H. Rackham, Trans., Voi. 1, p. 361, Heinemann, London, 1964.
3. Worcester, G. R. C., *Sail and Sweep in China*, HMSO, London, 1966.
4. Franklin, B., *Phil. Trans. Roy. Soc.* **64**, 445 (1774).
5. (a) Langmuir, I., *J. Am. Chem. Soc.* **39**, 1848 (1917). (b) *Trans. Faraday Soc.* **15**, 62 (1920).
6. Blodgett, K. B., *J. Am. Chem. Soc.* **57**, 1007 (1935).
7. Gaines, G. L., *Insoluble Monolayers at Liquid-Gas Interfaces*, Interscience, New York, 1966.
8. Ulman, A., *An Introduction to Ultrathin Organic Films: From Langmuir-Blodgett to Self-Assembly*, Academic Press, Boston, 1991.

9. (a) Tregold, R. H., *Rep. Prog. Phys.* **50**, 1609 (1987). (b) R. H. Tregold, *Order in Thin Organic Films*, Cambridge Press, Cambridge, 1994.
10. (a) Russell, T. P., *Mater. Sci. Rep.* **5**, 171 (1990). (b) M. Deutsch and B. Ocko, *X-ray and Neutron Reflectivity*, in *Encyclopedia of Applied Physics*, G. L. Trigg, Ed., VCH, New York, in press. (c) Als-Nielsen, J. and Kjær, K., in *Phase Transitions in Soft Condensed Matter*, T. Riste and D. Sherrington, Eds., p. 113-138, Plenum Press, New York, 1989. (d) Schlossman, M. L. and Pershan, P. S., in *Light Scattering by Liquid Surfaces and Complementary Techniques*, D. Langevin, Ed., p. 365-404, Marcel Dekker, New York, 1990.
11. (a) Wolf, S. G., Leiserowitz, L., Lahav, M., Deutsch, M., Kjær, K., and Als-Nielsen, J., *Nature* **328**, 63 (1987). (b) Kjær, K., Als-Nielsen, J., Fielm, C. A., Laxhuber, L. A., and Möhwald, H., *Phys. Rev. Lett.* **58**, 2224 (1987). (c) Dutta, P., Peng, J. B., Lin, B., Ketterson, J. B., Prakash, M., Georgopoulos, P., and Ehrlich, S., *Phys. Rev. Lett.* **58**, 2228 (1987).
12. (a) See review in ref. 9. (b) Als-Nielsen, J., Jacquemain, D., Kjær, K., Leveiller, F., Lahav, M., and Leiserowitz, L., *Phys. Rep.* **246**, 251 (1994). (c) Knobler, C. M., *J. Phys. Cond. Matt.* **3**, 1 (1991). (d) Rieu, J. P., Legrand, J. F., Renault, A., Berge, B., Vallade, M., Ocko, B. M., Wu, X. Z., and Deutsch, M., *J. Phys. (France) II* **5**, 607 (1995). (e) Bommarito, G. M., Foster, W. J., Pershan, P. S., and Schlossman, M. L., *J. Chem. Phys.* **105**, 5265 (1996). (f) Weinbach, S. P., Weisbuch, I., Kjær, K., Bouwman, W. G., Als-Nielsen, J., Lahav, M., and Leiserowitz, L., *Adv. Mater.* **7**, 857 (1995). (g) Foster, W. J., Shih, M. C., and Pershan, P. S., *J. Chem. Phys.* **105**, 3307 (1996).
13. (a) Bourdieu, L., Daillant, J., Chatenay, D., Braslau, A., and Colson, D., *Phys. Rev. Lett.* **72**, 1502 (1994). (b) Kent, M. S., Lee, L. T., Factor, B. J., Rondelez, F., and Smith, G. S., *J. Chem. Phys.* **103**, 2320 (1996). (c) Schlossman, M., Schwartz, D. K., Kawamoto, E. H., Kellog, G. J., Pershan, P. S., Kim, M. W., and Chung, T. C., *J. Phys. Chem.* **95**, 6628 (1991). (d) Bourdieu, L., Chatenay, D., Daillant, J., and Luzet, D., *J. Phys. (France) II* **4**, 37 (1994).
14. (a) Vaknin, D., Wang, J. Y., and Uphaus, R. A., *Langmuir* **11**, 1435 (1995). (b) Wang, J. Y., Vaknin, D., Uphaus, R. A., Kjær, K., and Lösche, M., *Thin Solid Films* **242**, 40 (1994). (c) Fukuto, M., Pennanen, K., Heilmann, R. K., Pershan, P. S., and Vaknin, D., *J. Chem. Phys.* **107**, 5531 (1997).
15. (a) Graner, F., Perez-Oyarzun, S., St.-Jalmes, A., Flament, C., and Gallet, F., *J. Phys. (France) II* **5**, 313 (1995). (b) Weinbach, S. P., Kjær, K., Bouwman, W. G., Grubel, G., Legrand, J. F., Als-Nielsen, J., Lahav, M., and Leiserowitz, L., *Science* **264**, 1556 (1994).
16. Bigelow, W. C., Pickett, D. L., and Zisman, W. A., *J. Coll. Interf. Sci.* **1**, 513 (1946).
17. (a) Netzer, L., and Sagiv, J., *J. Am. Chem. Soc.* **105**, 674 (1983). (b) Maoz, R., and Sagiv, J., *J. Coll. Interf. Sci.* **100**, 465 (1984).
18. Nuzzo, R. G., and Allara, D. L., *J. Am. Chem. Soc.* **105**, 4481 (1983).
19. For a recent excellent concise review see: Ulman, A., *MRS Bull.*, June 1995, p. 46.
20. Fenter, P., Eisenberger, P., Burrows, P., Forrest, S. R., and Liang, K. S., *Physics B* **221**, 145 (1996).
21. (a) Prime, K., and Whitesides, G. M., *Science* **252**, 1164 (1991). (b) Spaltenstein, A., and Whitesides, G. M., *J. Am. Chem. Soc.* **113**, 686 (1991).
22. (a) Small, D. M., *The Physical Chemistry of Lipids*, Plenum, New York, 1986. (b) Sirota, E. B., King Jr., H. E., Shao, H. H., and Singer, D. M., *J. Phys. Chem.* **99**, 798 (1995). (c) Craievich, A., Doucet, J., and Denicolo, I., *Phys. Rev. B* **32**, 4164 (1985).
23. (a) Wu, X. Z., Sirota, E. B., Sinha, S. K., Ocko, B. M., and Deutsch, M., *Phys. Rev. Lett.* **70**, 958 (1993). (b) Wu, X. Z., Ocko, B. M., Sirota, E. B., Sinha, S. K., Deutsch, M., Cao, G. H., and Kim, M. W., *Science* **261**, 1018 (1993). (c) Earnshaw, J. C., and Hughes, C. J., *Phys. Rev. A* **46**, R4494 (1992). (d) Deutsch, M., Wu, X. Z., Sirota, E. B., Sinha, S. K., Ocko, B. M., and Magnussen, O. M., *Europhys. Lett.* **30**, 283 (1995). (e) Wu, X. Z., Ocko, B. M., Tang, H., Sirota,

- E. B., Sinha, S. K., and Deutsch, M., *Phys. Rev. Lett.* **75**, 1332 (1995). (f) Wu, X. Z., Ocko, B. M., Sirota, E. B., Sinha, S. K., Gang, O., and Deutsch, M., *Phys. Rev. E* **55**, 3164 (1997).
24. Weast, R. C., Astle, M. J., and Beyer, W. H., Eds., *CRC Handbook of Chemistry and Physics*, 66th ed., p. F174-F184, CRC Press, Boca Raton, FL, 1986.
25. (a) Rappe, A. K., et al., *J. Am. Chem. Soc.* **114**, 10024 (1992). (b) *Cerius2: Molecular Modeling Software*, Molecular Simulations Inc., Cambridge, UK.
26. Zangwill, A., *Physics at Surfaces*. Cambridge University Press, Cambridge, 1988.
27. Smith, T., *Adv. Coll. Interf. Sci.* **3**, 161-221 (1972).
28. De Levie, R., *Chem. Rev.* **88**, 599-609 (1988).
29. Buess-Herrman, C., *Prog. Surf. Sci.* **46**, 335-375 (1994).
30. Demoz, A., and Harrison, D. J., *Langmuir* **8**, 1046-1050 (1993).
31. Turyan, I., and Mandler, D., *Analy. Chem.* **66**, 58-63 (1994).
32. Bruckner-Lea, C., Kimmel, R. J., Janata, J., Conroy, J., and Caldwell, K., *Electrochem. Acta.* **40**, 2897-2904 (1995).
33. (a) Bruckner-Lea, C., Janata, J., Conroy, J., Pungor, A., and Caldwell, K., *Langmuir* **9**, 3612 (1993). (b) Conroy, J., and Janata, J., *Appl. Phys. Lett.* **68**, 569-571 (1996). (c) Conroy, J., Caldwell, K., Bruckner-Lea, C., and Janata, J., *J. Phys. Chem.* **100**, 18,222-18,228 (1996). (d) Conroy, J., Hlady, V., Bruckner-Lea, C., and Janata, J., *J. Phys. Chem.* **100**, 18,229-18,233 (1996).
34. Magnussen, O. M., Ocko, B. M., Regan, M. J., Penanen, K., Pershan, P. S., and Deutsch, M., *Phys. Rev. Lett.* **74**, 4444 (1995).
35. Barton, S. W., Thomas, B. N., Novak, F., Weber, P. M., Harris, J., Dolmer, P., Bloch, J. M., and Rice, S. A., *Nature* **321**, 685 (1986).
36. Regan, M. J., Kawamoto, E. H., Lee, S., Pershan, P. S., Maskil, N., Deutsch, M., Magnussen, O. M., Ocko, B. M., and Berman, L. E., *Phys. Rev. Lett.* **75**, 2498 (1995).
37. Flom, E. B., Li, M., Acero, A., Maskil, N., and Rice, S. A., *Science* **260**, 332 (1993).
38. (a) Regan, M. J., Pershan, P. S., Magnussen, O. M., Ocko, B. M., Deutsch, M., and Berman, L. E., *Phys. Rev. B* **55**, 15874 (1997); (b) Lei, N., Huang, Z. Q., and Rice, S. A., *J. Chem. Phys.* **107**, 4051 (1997); *J. Chem. Phys.* **105**, 9615 (1996).
39. Regan, M. J., Tostmann, H., Pershan, P. S., Magnussen, O. M., DiMasi, E., Ocko, B. M., and Deutsch, M., *Phys. Rev. B* **55**, 10786 (1997).
40. (a) Ocko, B. M., Wu, X. Z., Sirota, E. B., Sinha, S. K., and Deutsch, M., *Phys. Rev. Lett.* **72**, 242 (1994). (b) Rowlinson, J. S., and Widom, B., *Molecular Theory of Capillarity*, Clarendon, Oxford, 1982. (c) Buff, F. P., Lovett, R. A., and Stillinger, F. H., *Phys. Rev. Lett.* **15**, 621 (1965). (d) Sengers, J. V., and van Leeuwen, J. M. J., *Phys. Rev. A* **39**, 6346 (1989). (e) Gelfand, M. P., and Fisher, M. E., *Physica A* **166**, 1 (1990).
41. Barton, S. W., Thomas, B. N., Flom, E. B., Novak, F., and Rice, S. A., *Langmuir* **4**, 233 (1988).
42. Harzallah, B., Bosio, L., Cortes, R., and Errafii, N., *J. Chim. Phys. (Paris)* **93**, 1202 (1996).
43. Magnussen, O. M., Ocko, B. M., Deutsch, M., Regan, M. J., Pershan, P. S., Berman, L. E., Abernathy, D., Legrand, J. F., and Grübel, G., *Nature* **384**, 250 (1996).
44. Pershan, P. S., and Als-Nielsen, J., *Phys. Rev. Lett.* **52**, 759 (1984).
45. Fraser, K. A., et al., *Acta Cryst. C* **51**, 406 (1995).
46. Laibinis, P. E., and Whitesides, G. M., *J. Am. Chem. Soc.* **114**, 9022 (1992).
47. Fenter, P., Eisenberger, P., and Liang, K. S., *Phys. Rev. Lett.* **70**, 2447 (1993).
48. Strong, L., and Whitesides, G. M., *Langmuir* **4**, 546-558 (1988).
49. Chidsey, C. E. D., Liu, G., Rowntree, Y. P., and Scoles, G., *J. Chem. Phys.* **91**, 4421 (1989).
50. Weinbach, S. P., Jacquemain, D., Leveiller, F., Kjær, K., Als-Nielsen, J., and Leiserowitz, L., *J. Am. Chem. Soc.* **115**, 11,110 (1993).